Journal of Applied Polymer Science

Needle-Punched Nonwoven Matrix from Regenerated Collagen Fiber for Cartilage Tissue Engineering

Nanfei He,[1] Qinfei Ke,[1,2] Chen Huang,[1] Jun Yang,[2] Yaping Guo[2]
[1]College of Textiles, Donghua University, Shanghai 201620, People's Republic of China
[2]Deparment of Chemistry, Shanghai Normal University, Shanghai 200234, People's Republic of China
Correspondence to: Q. Ke (E-mail: kqf@dhu.edu.cn)

ABSTRACT: In this study, a new application of needle-punched three-dimensional (3D) fiber matrix from regenerated collagen fiber in articular cartilage tissue engineering (TE) was developed. Scanning electron microscopy images showed that the arrangement of fibers well mimicked the transitional part of the zonal articular cartilage. The 3D matrices exhibited a high porosity (93.5 ± 2.3%) and a large pore size range from about 20 μm in the inner part to 200–300 μm on the surface. The interconnected pore structure and hydrophilicity of the fibers led to the rapid and desired water uptake capacity of the matrices. Although the tensile and compressive properties of the scaffold were slightly lower than those of the natural articular cartilage, the anisotropic and nonlinear tension–compression were highly similar. *In vitro* human bone marrow stromal cells proliferation and cell morphology revealed the well cytocompatibility of the matrix, indicating its great potential in articular cartilage TE. © 2014 Wiley Periodicals, Inc. J. Appl. Polym. Sci. **2014**, *131*, 40404.

KEYWORDS: biomedical applications; biomaterials; fibers; morphology

Received 21 October 2013; accepted 5 January 2014
DOI: 10.1002/app.40404

INTRODUCTION

The main function of articular cartilage, a smooth wear-resistance tissue lining at the ends of bones, is to support and transmit applied loads and functions biomechanically as a multiphasic fiber-reinforced material.[1,2] Because of the avascular nature of cartilage, poor nutrition supply (e.g., oxygen and glucose), and insufficient removal of metabolic waste (e.g., lactate),[3–5] it is extremely difficult to repair and regenerate injured or diseased articular cartilage through natural healing.[6] Until now, there is still no entirely satisfactory clinical solution to restore long-term function.[7,8]

Tissue engineering (TE) combines three-dimensional (3D) scaffolds, cells, and signaling molecules to serve as an alternative treatment for cartilage defects.[9–11] Scaffold plays an essential role in guiding the formation of new tissue. Typical articular cartilage tissue consists of four, spatially distinct zones (the superficial, transitional, deep, and calcified zones) and exhibits anisotropic, heterogeneous, nonlinear tension–compression in terms of biomechanical properties.[2,12] In addition, pore size, porosity, pore interconnectivity, scaffold surface area, and scaffold material are all critical factors that can influence chondrocyte biology.[13] Ideally, the scaffold architecture should possess suitable mechanical properties and favorable pore structure to closely mimic the naturally texture.[14]

Fibrous scaffolds normally have large surface area and volume, homogeneous fiber size and a wide range of pore distribution, which make them favorable for TE.[15] Different fabrication techniques have enabled the development of various fibrous matrices, including braided, knitted, woven, and nonwoven matrices. In particular, nonwoven fibrous matrices are most promising tissue replacement materials because of their special porous structure and simple manufacturing process.[16]

Broadly speaking, nonwovens are flat, flexible, porous sheet, or web structures bonded together by entangling fiber or filaments mechanically, thermally, or chemically.[17] In the recent years, nanofiber nonwovens from electrospinning have been extensively studied.[18] However, such scaffold is too thin that is prone to be a 2D dimension on a macroscale with small pores ($<$50 μm), whereas the thickness of articular cartilage varies from $<$500 μm to 7.1 mm[19,20] and the favorable pore diameter diverse from 100 to 500 μm.[21,22]

In comparison with electrospinning, needle punching shows promising ability in producing reproducible 3D fibrous matrices with interconnected pores and controlled structure. This is a process for converting fiber webs into coherent fabrics, normally by means of repeated penetration of a set of barbed needles, which produce mechanical bonds within the web.[23,24] In addition, needle punching is a simple and affordable manufacturing process. All pores in this needle-punched scaffold (NPS) are

naturally connected that is advantageous in pore interconnectivity. In addition, NPS usually have a high porosity and large surface areas.[25] Both the productivity and the porous structure make the NPS a promising scaffold in medical fields such as bone tissue, heart valves, and blood compatible interfaces.[26–28]

An excellent scaffold should not only mimic the structure of the articular cartilage but also the cartilage composition. It is reported that collagen (Type II) accounts for about 60% of the dry weight of adult articular cartilage.[29] Therefore, the usage of collagen materials as components of scaffold would be favoring in enhancing chondrogenesis. Regenerated collagen fibers (RCFs, Type II) deriving from animals have excellent biodegradability, low antigenicity, and cell-binding properties.[30]

In this work, the needle-punched process was used to produce RCF 3D porous scaffolds used in articular cartilage TE. Both the structure and physicochemical properties of the scaffolds well mimic the native cartilage. The cell proliferation assay and phenotypes observation show the scaffolds have a good cytocompatibility.

EXPERIMENTAL

RCFs (length 38 mm) were purchased from Shanghai Quanyu Biotech Suiping Co. (Shanghai, China). All solvents were purchased from Sigma-Aldrich (St. Louis, MO), unless stated otherwise.

Measurement of Material

Fiber properties were measured according to the standards (ISO 137: 1975, ASTM D3822-2007, ASTM D3937-2007). The average diameter of collagen fiber was calculated using an automatic fiber testing system (Beion F10; Beion Co., LA) by randomly selecting 300 fiber strands. Single fiber tensile tests were performed by a fiber tensile tester (XQ-2; Shanghai New Fiber Instrument Co., Shanghai, China) at a gauge length of 10 mm and a drawing speed of 10 mm min^{-1} under both dry and wet state. The crimping of fiber and fiber crimp stability were determined using a fiber crimp elasticity tester (YG362B; Changzhou The Second Textile Machines Co., Jiangsu, China).

Fabrication of Scaffold

The RCF scaffold was produced by needle punching process. Briefly, a fibrous web was prepared from collagen staple fibers using a laboratory carding machine (ASI8IA; Jiangxi Textile Equipment Co., Jiangxi, China). Most of the fibers were arranged along the machine direction (MD). Seven or eight layers of the carded webs were parallel layered before subjected to a needle machine (F22G-I1600; Changshu Weicheng NonWoven Equipment Co., Jiangsu, China) equipped with 4,500 needles (15 × 18 × 32 × 3 R333 G3027; Groz-Beckert, Albstadt, Germany) per running meter to obtain the nonwoven fabrics with a needle punching density of 428 lp cm^{-2}. And the depth of needle penetration was 6 mm. The process was shown in Figure 1.

Characterization of the RCF NPSs

Morphology and Structure Analysis. Measurement of thickness and surface weight of NPSs were carried out, respectively, on a digital fabric thickness gauge (YG141N; Nantong Hongda Experiment Instruments Co., Jiangsu, China) and electronic balance (FA2004N; Shanghai Jinghua Technology Instrument Co., Shanghai, China).

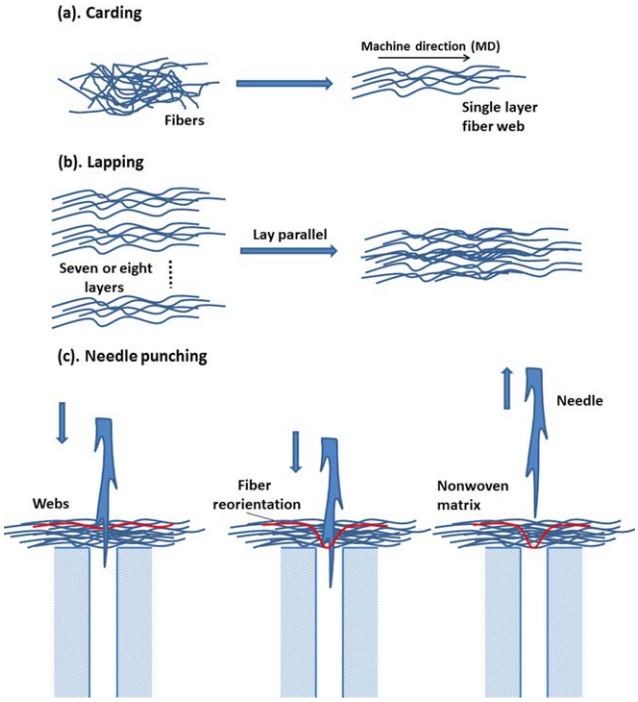

Figure 1. Schematic diagrams of needle punching process. (a) Carding, preparation of single-layer fiber web. (b) Lapping, obtaining the web with certain area density to fit the requirement of needle punching. (c) Needle punching, consolidating the NPS. [Color figure can be viewed in the online issue, which is available at wileyonlinelibrary.com.]

The surface and cross-section of the NPSs were visualized by scanning electron microscope (JSM-5600LV; JEOL, Tokyo, Japan) at an accelerating voltage of 10 kV. For the cross-section analysis, the sample was fractured in liquid nitrogen before cutting. Before scanning electron microscopy (SEM) observation, all the samples were coated with a thin layer of sputtered gold. In addition, RCFs stained by phalloidin was observed on a laser scanning confocal microscope (LSCM, Leica TCS SP2; Leica Microsystem, Heidelberg, Germany) to visualize the 3D structure of the NPS.

For the NPS with a certain thickness (about 3–4 mm), pore size changes considerably along thickness direction [e.g., Figure 2(a)].[31] Therefore, we combined the image analysis and the capillary flow porosimetry (CFP, Through-pore Size Analyzer, Porometer 3G zh; Quantachrome Instruments, FL) to characterize considerably more information about the through pore structure. The SEM and LSCM images of the scaffold yielded surface information [pore size in Figure 2(a), part A] about the through pore. The CFP test measured the constricted part of the through pore [pore size in Figure 2(a), part B].

CFP provides a nondestructive and simple technique that allows accurate and rapid measurement of pore size and distribution.[18] However, this method tests only the throat diameter of each through pore [32] [Figure 2(a), part B]. During the CFP measurement, the pores of the sample were first filled with a wetting

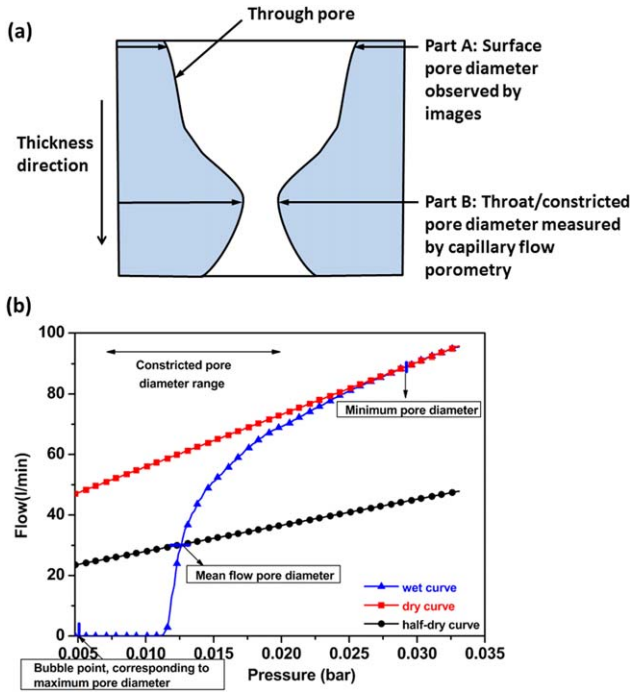

Figure 2. (a) Schematic diagram of a typical through pore of the NPS and (b) typical results of CFP obtained from the needle-punched nonwoven (1 bar = 100 kPa). The mean flow pore diameter is calculated at the intersection of half dry-flow data set with the wet flow data. [Color figure can be viewed in the online issue, which is available at wileyonlinelibrary.com.]

liquid, the pororil wetting fluid of a defined surface tension of 16 dynes cm^{-1} (Quantachrome Instruments), then the liquid was emptied by a nonreacting pressurized gas. After all the liquid was extruded from the pores, gas blew through the same dry sample. The differential pressures and gas flow rates through wet and dry samples were measured and the results were shown in Figure 2(b). From data plotted in these two curves, the pore size (maximum, minimum pore diameter, and mean flow pore diameter which often corresponds to the peak of the pore size distribution) and distribution were calculated by the software from Quantachrome Instruments using the following equation[31]:

$$D = \frac{4\gamma\cos\theta}{\Delta p} \quad (1)$$

where D is the pore diameter, γ the surface tension of the wetting liquid, θ the contact angle of the wetting liquid, and Δp is the differential pressure.

The open porosity can be calculated by the liquid displacement method. The NPSs (2 cm × 2 cm) with known dry weight (W1) was submerged in a known density (ρ) of liquid that was not a solvent for the scaffold. The surface tension of the liquid was low, thus made the scaffold easy to be completely soaked. Then the wet scaffold was weighted (W2) and the porosity was calculated by the following equation:

$$\text{Porosity} = \frac{100\times(\text{W2}-\text{W1})}{\rho\times\text{Vs}} \quad (2)$$

where Vs is the apparent (total) volume of a porous material. The total volume was obtained by determining the scaffold side length and thickness, assuming that a cubic scaffold was constructed ($n = 10$).

Surface Wettability. The contact angle of the NPS was measured by a static contact angle (OCA15EC; DataPhysics Instruments GmbH, Filderstadt, Germany). Five samples ($n = 5$) were used for each test.

Attenuated Total Reflectance Fourier Transform Infrared Analysis. Attenuated total reflectance (ATR) Fourier transform infrared (FTIR) spectra were performed by a FTIR-Raman (Nexus 670; Thermo Fisher Nicolet Co., MA) after desiccation over a range of 4,000–800 cm^{-1} to investigate the possible chemical properties of collagen scaffold.

Water Uptake. The ability of the NPSs to absorb water was studied to understand the water holding capability as well as the stability of scaffold in water. The water uptake was obtained as follows, the NPSs (2 cm × 2 cm) with known dry weight (W0) were placed in phosphate-buffered saline (PBS, PH 7.4) at 37°C for 30 min, 2 h, 4 h, 6 h, and 8 h. Then the medium was carefully withdrawn at intervals and wet weight of the scaffolds was measured until equilibrium in weight was attained (Wt). Water uptake was calculated using the following formula:

$$S = \frac{\text{Wt}-\text{W0}}{\text{W0}} \quad (3)$$

where S is the percentage of water uptake ability, Wt denotes the weight of the scaffolds at time t, and W0 is the initial weight of the scaffolds.

Mechanical Tests. In this study, both tensile and compressive mechanical properties were measured using an electromechanical universal testing machine (WDW-20; Shanghai Hualong Test Instruments Co., Shanghai, China). To simulate the *in vivo* condition, the samples were tested in hydrated state by immersing them into PBS for 2 h in a water bath at 37°C.

For tensile tests, NPSs were cut into rectangular specimens ($n = 5$) of 60 mm long and 20 mm wide and were stretched to break under a constant crosshead speed of 10 mm min^{-1} and a gauge length of 40 mm. Ultimate tensile strength (UTS) was calculated at the maximum load immediately before breaking. Young's modulus was determined from the slope of the linear segment of the stress–strain curve. Both the specimens along the MD and cross-machine direction (CD) were tested.

Compression experiment was carried out in an unconfined-compressing configuration. The NPSs were cut into 2 cm × 2 cm and the compression speed was 0.5 mm min^{-1}. Compressive modulus was also determined based on the slope of the entire linear elastic region of the stress–strain curve.

Cell Culture. Human bone marrow stromal cells (hBMSCs; Lonza, Walkersville, MD) were cultured in α-modified minimum essential medium (α-MEM) containing 10% fetal bovine serum (FBS), 1% penicillin (100 U mL^{-1}), and streptomycin sulfate (100 mg mL^{-1}). The samples were incubated at 37°C in a humidified atmosphere containing 5% CO_2, with the growth medium changed every 2 days. For cell seeding, NPSs (15 mm in diameter) were sterilized under UV radiation and washed with PBS three times. Then the hBMSCs were seeded at a

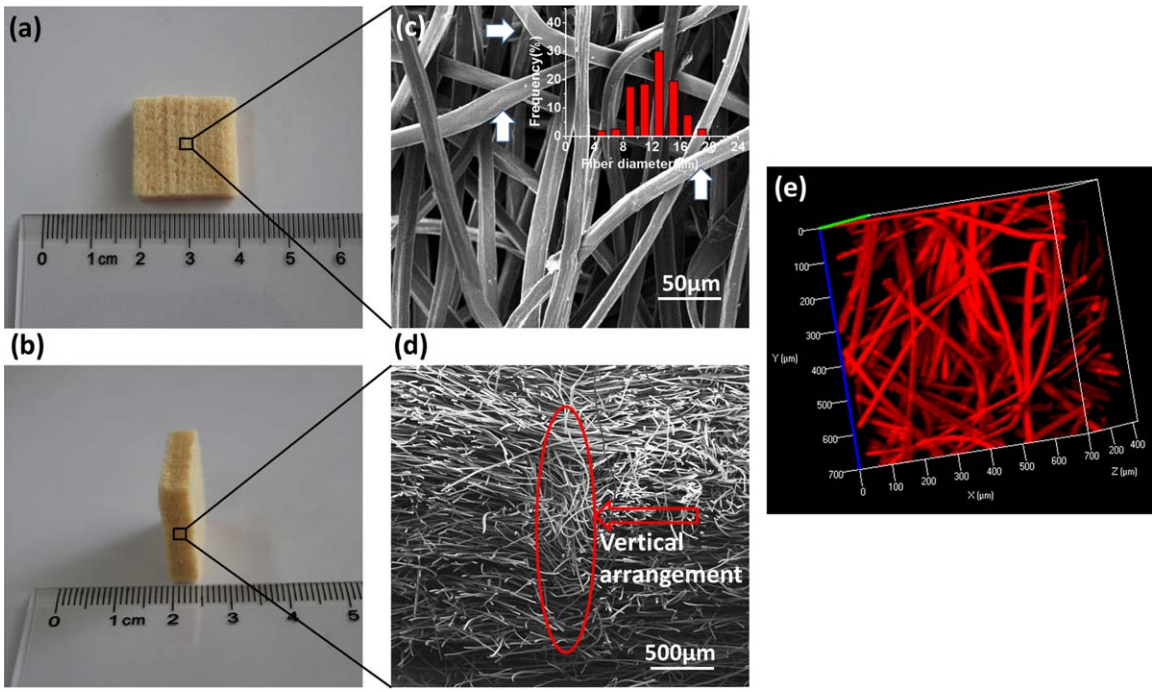

Figure 3. (a) Surface and (b) cross-section photos of the RCF NPS (2 cm × 2 cm and 4.74 ± 0.35 mm thickness). (c) Surface and (d) cross-section SEM images of the RCF NPS. (e) 3D LSCM micrograph of NPS, the RCFs were stained by phalloidin. [Color figure can be viewed in the online issue, which is available at wileyonlinelibrary.com.]

density of 2×10^4 cells per well in 24-well plates and cultured in the α-MEM medium containing 10% FBS.

Cell Proliferation. The cell proliferation was qualified by cell counting kit 8 (CCK-8 kit; Beyotime, Shanghai, China) after seeding for 1 day, 3 days, 5 days, and 7 days. At desired time points, the CCK-8 solution was added to each well, followed by incubation for 2 h with 5% CO_2 at 37°C. Afterward, the supernatant solution was transferred into a 96-well plate, and the optical density was observed at 450 nm by a microplate reader (Bio-RAD680; Bio-Rad Co., CA).

Cell Morphology. hBMSCs morphology on RCF NPSs was evaluated by LSCM. After 24 h of culture, hBMSCs were washed with PBS, fixed in 4% paraformaldehyde for 10 min, and immersed in 0.1% Triton X solution for 15 min. Tetramethylrhodamine (TRITC)-phalloidin was used to stain actin filaments and 4′,6-diamidino-2-phenylind (DAPI) was used to stain nuclei. The mounted samples were observed and viewed by LSCM.

Statistical Analysis. All data were expressed as mean ± standard deviation. Statistical analysis was performed using analysis of variance.

RESULTS AND DISCUSSION

Evaluation of Material Properties

The physical properties of the RCFs play an essential role in needle-punched process and could also influence the structure of final scaffold.[33]

The average diameter of RCFs was 12.48 ± 2.79 μm and the diameter distribution was shown in Figure 3(a). The degree of fineness is supposed to be suitable for needle punching and is close to the ultrafine fiber (<10 μm).[34] Generally, at same surface density, the finer the fibers are, the higher the specific surface area would be.[35] More contact points and areas will also be created among fibers, which could definitely increase the slip resistance between fibers and then enhance the strength. However, when take processing technique and cells culture into consideration, the fiber should not be too fine so as to withstand the mechanical effect and be conducive to cell (diameter around 10 μm in our study) adhesion and proliferation in terms of surface area.[36,37] Consequently, the fiber we used offers a comparatively high specific surface area and is proper for processing and the cells growth.

The tensile strength of RCFs was 515.28 ± 99.55 N mm^{-2} in dry condition, 492.38 ± 82.04 N mm^{-2} in wet condition. The strain at failure was 18.79 ± 3.19% in dry condition and 16.61 ± 2.57% in wet condition. No significant differences were found among dry and wet state.

Curl of RCFs refers to its degree of curvature, is another important structural parameter which could exert a critical influence on the initial modulus of a nonwoven fabric.[38] The crimp frequency and crimp ratio of RCF were 7.75 ± 2.31 crimps cm^{-1} and 6.19 ± 2.80%, respectively. Compared to many other rayon, the crimp characteristics of this RCF was in a comparative high level[39] which could contribute to the carding process and facilitate the entanglement between fibers.[40]

Characterization of Scaffold Morphology and Structure

The thickness of NPS was 4.74 ± 0.35 mm and the surface density was 444.12 ± 31.57 g m^{-2}. During the process of needle punching, the desired thickness and surface density can be obtained by adjusting layers of fiber webs, depth of penetration, and punching

density.[24] Figure 3(a,b) provided a macroscopic appearance of this scaffold. Furthermore the surface and cross-section microstructure of NPSs were exhibited in the SEM images [Figure 3(c,d)] and the LSCM micrograph [Figure 3(e)] showed the 3D structure of the scaffold. Most part of the fibers is arranged parallel to the MD because of the carding and lapping process [Figure 1(a,b)]. Meanwhile, due to the penetrating action of barbed needles [Figure 1(c)] and the drafting effect during the needle-punching process, partial few fibers reorientated and intermingled from horizontal direction to the CD [Figure 3(c), arrows] or a vertical direction [Figure 3(d)]. Such orientation and interlocking of the fibers that created and reinforced this kind of scaffold. Fiber orientation is a primary factor influencing the tensile strength of the nonwoven material. The tensile strength was better in MD because the majority of fibers were arranged along this direction. Correspondingly, elongation was higher in the CD. Moreover, the difference in tensile strength between MD and CD could be adjusted through altering the web-laying technique from parallel-laid to cross-laid or random-laid.[33]

One of the most exceptional characteristics of articular cartilage structure is the zonal variations in the organization of the collagen network. In the superficial zone, the collagen fibrils oriented tangentially to the articular surface. The middle zone contains randomly oriented collagen fibers and provides a transition to the low or deep zone in which the fibers aligned in a columnar fashion.[38,39] Although the NPS did not possess the same structure as the zonal articular cartilage, it still showed much resemblance. Specifically, the parallel arrangement fibers mimicked the collagen fibrils in the surface layer of the articular cartilage; the perpendicular distribution fibers corresponded to cartilage's columnar structure; and the other reoriented fibers imitated the randomly distribution part. So in general, the fiber orientation in the matrix could well mimic the middle zone of articular cartilage transition from the superficial zone to the deep zone. It is also worthy to mention that the number of vertical arrangements of fibers increases with the rising of needle punch density.[41]

Pore size, porosity, and pore interconnectivity play a crucial role in cell migration and diffusion of nutrients, oxygen, waste products, and signaling molecules.[37] A wide range of pore sizes are considered acceptable in cartilage TE.[42] The optimal pore sizes need to be large enough to allow cell migration, but also small enough to establish a sufficiently high specific surface area for cell adhesion.[43] A study recommended pores smaller than 50 μm could help to improve biomechanical strength of engineered constructs.[44]

Pores in NPS are interconnected and irregular, they various along the thickness direction [Figure 3(e), z axis]. Generally the pore size in the surface layer of the scaffold is always larger than the rest part of the through pore. From the SEM image showing the surface in Figure 3(c) and LSCM image showing around 200 μm from the surface in Figure 3(e), it was clear that the diameters of many pores in the surface layer could reach 200–300 μm, or even larger. While according to the CFP technique, the constricted pore diameter of the scaffold ranged from 22.122 μm to 129.817 μm. Its distribution was illustrated in Figure 4, with mean flow diameter of 50.473 μm. Therefore,

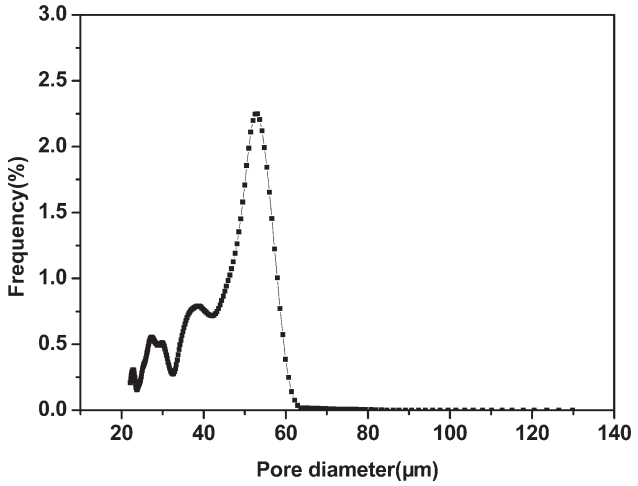

Figure 4. Pore size distribution of the needle-punched scaffold.

it can be seen that the needle punching process provide a fiber matrix with wide range pore size. The larger pores in the superficial zone of the NPS could induce the passive cell distribution while seeding that is to say cell infiltration. And the smaller pores inner the matrix also means the small distance between fibers but still several times larger than the size of cells, might weaken the passive cell distribution but would not hamper the active distribution by cell movement.[37] Besides, they could contribute to maintain the biomechanical of the scaffold.

As expected, the fibrous matrices had a high porosity about $93.5 \pm 2.3\%$, providing NPS a great advantage when compared to the other methods as solid freeform fabrication (55–70%)[14] and 3D weaving (~74%).[2] Another distinguished feature of NPS is the high level of pore interconnectivity. These features ensure large pore space and better supply of oxygen and nutrients for cells to proliferation. Pore structure has strong dependence on needle-punched process variables.[45] Generally, with an increase in needle punch density by improving stroke frequency or reducing feed roller speed, the pore size, and porosity of the NPS will decrease correspondingly because the matrix structure tends toward higher degree of consolidation.[24,46]

To sum up, all the above structure performances can be adjusted by changing needle punch processing parameters, such as the depth of needle penetration, average feed roller speed, stroke frequency, the number of carded fiber web, and web arrangement pattern.

Chemical Composition and Water Uptake Ability

The characteristic of hydrophilicity is critical to cartilage scaffold as it could enhance the cell viability and proliferation.[47]

The static contact angle of the fiber matrices is $44.48 \pm 5.87°$, indicating that the RCF NPS possessed an excellent hydrophilicity. Figure 5(a) is the ATR-FTIR spectrum of RCF NPS. The characteristic peak at 1,658 cm^{-1} represents C=O stretching vibration of amide I band. Corresponding to the coupling of bending of N-H bond and stretching of C-N bonds, the peaks at 1,542 cm^{-1} and 1,237 cm^{-1} are amide II band and amide III

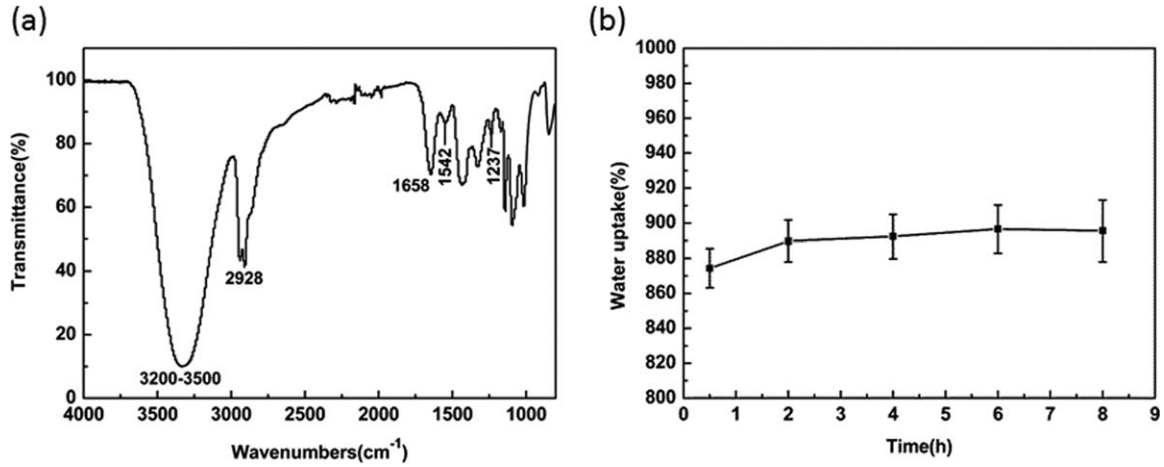

Figure 5. (a) ATR-FTIR spectra of RCF NPS. (b) Water uptake ratio versus time for the RCF NPS.

band. Moreover, the broad band between 3,500 cm^{-1} and 3,200 cm^{-1} represents the aliphatic –OH stretching. The peak at the frequency of 2,928 cm^{-1} was owing to the aliphatic side chains present in the collagen backbone. Water uptake capacity was measured and presented in Figure 5(b). It was evident that the fiber matrices could absorb a large amount of water and attained water uptake equilibrium rapidly.

The rapid and large amount water uptake capability of the fiber matrices could be attributed to their special structure and the surface chemical property. The collagen fiber is abundant with hydrophilic groups as illustrated from the ATR-FTIR spectrum, such as hydroxyl, amino and carboxyl groups, which can be easily hydrated with water. The large number of narrow pores in the scaffold might also entrap and hold more water though capillary action.[48] High water uptake indicates the ability to carry out as a good fiber matrix for cartilage regeneration to ensure the substance exchange. The ability of holding large amounts of medium may help in free diffusion of nutrients (e.g., oxygen) that could help maintain cell viability and promote secretion of extra cellular matrix.[9,49] Furthermore, it could also influence the mechanical behavior of the biomaterials.[30] Accordingly, the collagen fiber NPS is favorable for the cartilage TE with the respect of the water uptake ability.

Mechanical Properties

The mechanical properties of scaffolds for cartilage TE are of great importance. Scaffolds should be able to fulfill the requirement of stress imposed on it during *in vitro* culture and *in vivo* implantation.

For tensile test, ultimate tensile stress, strain and Young's modulus were calculated and shown in Table I. Testing of samples in MD versus CD resulted in high ultimate tensile stress and Young's modulus but low in ultimate tensile strain. The anisotropic mechanical properties were obvious when the scaffolds were tested along parallel (MD) and perpendicular (CD) to the predominant orientation of the fibers. Both UTS and Young's modulus at parallel direction were twice as high as those of perpendicular direction. Mature articular cartilage showed significant anisotropy in tension due to the preferred orientation of collagen fibers in the different zone of this structure.[50–52] As a result, the NPS in our study with multidirectional biomechanical behavior well mimicked the anisotropy of native cartilage.

Results from compression testing were also shown in Table I. The typical stress–strain curve was presented in Figure 6. No yield strength for the fibrous matrix was found because the stress versus strain curves did not show any evidence of yield, even after 25% of strain. In addition, the articular cartilage has approximately two orders of magnitude difference between the tensile and compressive modulus, demonstrating a high degree of tension–compression nonlinearity.[53] The scaffold we produced also presented this nonlinear property, which is believed to play a great role in its load-bearing capacity by enhancing

Table I. Tensile and Compressive Properties of NPSs versus Natural Articular Cartilage

	Scaffold		
	MD	CD	Articular cartilage
Tensile properties			
Ultimate tensile stress (MPa)	2.36 ± 0.22	1.24 ± 0.18	0.8–35[48,49,55]
Ultimate tensile strain (%)	57.27 ± 3.29	67.44 ± 9.73	10–40[48,49,55]
Tensile modulus (MPa)	1.73 ± 0.49	0.86 ± 0.07	5–25.5[50,56]
Compressive property			
Compressive modulus (MPa)	0.077 ± 0.023		0.24–0.85[54,57,58]

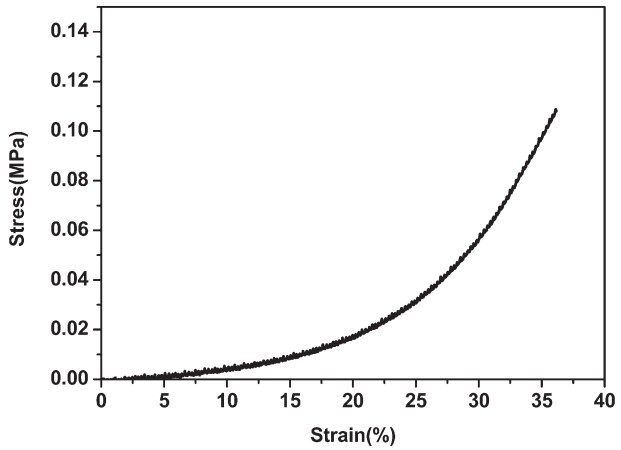

Figure 6. Typical compressive stress–strain curve of the NPS.

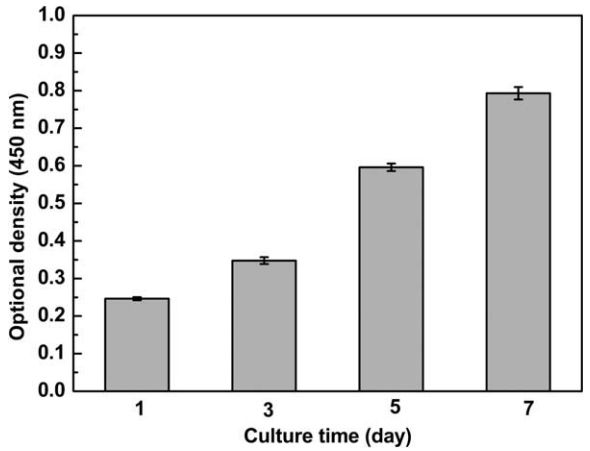

Figure 7. Cell proliferation (450 nm) varied with the culture time (mean ± SD).

the interstitial fluid pressurization and affect the transport of solutes.

As the strength of RCFs is relatively low (see material properties part) and needle-punched nonwoven may also possess a comparatively low strength due to the priority to have large pores, the mechanical properties of this scaffold is slightly lower than that of the nature articular cartilage, but still in the same order of magnitude. Furthermore, when the scaffold is deposited of an extracellular matrix (ECM) by cells, the tensile and compressive properties may be further improved.[54]

To sum up, although the tensile and compressive properties of the NPS are lower than those of the nature articular cartilage, they could have a further improvement by incorporation with an ECM. The scaffold could well simulate the anisotropic and tension–compression nonlinear properties of the nature articular cartilage.

Evaluation of *In Vitro* hBMSC Proliferation and Phenotype

The scaffold could provide a favorable matrix for the cell adhesion and proliferation because it physically mimicked ECM of native articular cartilage in terms of both composition and structure. Specifically, the scaffold simulated the zonal architecture of cartilage tissue, the anisotropic and nonlinear properties. Its suitable pore size, high porosity, and pore interconnectivity were also desirable in soft tissue repair. In this article, we studied the viability of hBMSCs onto the NPS using CCK-8 assay.

The cells proliferation results at Days 1, 3, 5, and 7 are showed in Figure 7. It is obvious that the optional density increased with the increase in culture time, suggesting good cell adhesion and proliferation on the NPS. During the first 5 days of cultivation, the proliferation rate kept on the rise, whereas after Day 5 it began to slow down. This might be ascribed to the culture system. In our study, the 3D cellular constructs were grown in static culture. It has been reported that the culture system that provided dynamic medium flow conditions could enhance nutrient exchange and hence increased cell viability and proliferation, especially in the center of the scaffold.[59] In a static environment, the cells initially were viable and proliferate readily on the outer surface of the 3D matrix. Although as more cells began to be clustered outside and cells within the construct may be less active or necrotic, then a lower proliferation rate was observed. A 3D perfusion tissue culture system will be developed in our future research to enhance mass transport and deliver controlled mechanical stimuli.

To observe the expressions of the cytoskeleton proteins of hBMSCs and the relationship between the cytoskeleton proteins and topographies of the fiber matrix, an immunocytochemistry staining and LSCM observation was performed on the cell

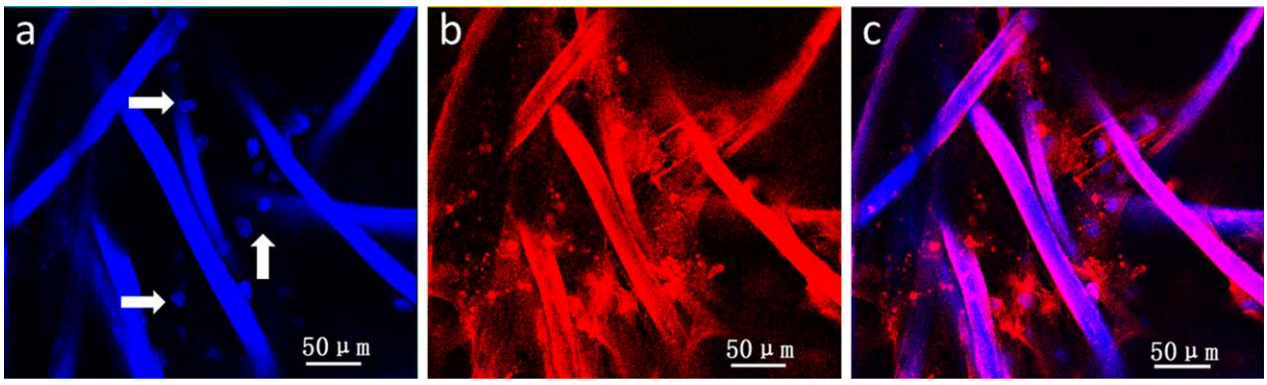

Figure 8. Representative LSCM images of cytoskeletal morphology of hBMSCs on RCF NPS (a–c) after 24 h of culture. [Color figure can be viewed in the online issue, which is available at wileyonlinelibrary.com.]

cultured at 24 h. Figure 8 shows the LSCM images of cytoskeletal morphology of hBMSCs on collagen fiber scaffold. The collagen fiber was blue in Figure 8(a) and red in Figure 8(b) because collagen could also be stained by DAPI and TRITC phalloidin. The white arrows indicate the cells' nuclei that were growing on the fibers at various depth of the matrix. From Figure 8(b) we can see the shape and direction of hBMSCs exhibited a fusiform-shaped morphology. Most of the cells spread along the direction of the fiber channel to show a 3D growth. Both CCK-8 assay and the LSCM images demonstrated that the NPS held a good cellular compatibility.

CONCLUSIONS

In this study, we fabricated RCF scaffold using needle punching process and evaluated its feasibility for articular cartilage TE. This 3D scaffold showed morphological similarities to the zonal organization of native articular cartilage, characterized by a wide range of pore sizes, high porosity, and pore interconnectivity. It also possessed well water uptake capability and suitable biomechanics (anisotropic, nonlinear mechanical properties). The cell studies using hBMSCs suggested that the scaffold is biocompatible and conducive to cell growth. Therefore, this kind of scaffold can be a good candidate for cartilage TE purpose. More evaluation about the biocompatibility and immunological reaction of the fibrous matrix *in vitro* or *in vivo* will be demonstrated in our further work.

ACKNOWLEDGMENTS

We are grateful to Dr. Teng Long for valuable assistance *in vitro* cell biocompatibility assessment. This research was supported by State Key Laboratory for Modification of Chemical Fibers and Polymer Materials, Dong Hua University.

REFERENCES

1. Lee, C.; Grad, S.; Wimmer, M.; Alini, M. *Top Tissue Eng.* **2005**, *2*, *1*.
2. Moutos, F. T.; Freed, L. E.; Guilak, F. *Nat. Mater.* **2007**, *6*, 162.
3. Huang, C. Y.; Gu, W. Y. *J. Biomech. Eng.* **2007**, *129*, 423.
4. Grimshaw, M. J.; Mason, R. M. *Osteoarthr. Cartil.* **2000**, *8*, 386.
5. Obradovic, B.; Carrier, R. L.; Vunjak-Novakovic, G.; Freed, L. E. *Biotechnol. Bioeng.* **1999**, *63*, 197.
6. Izadifar, Z.; Chen, X.; Kulyk, W. *J. Funct. Biomater.* **2012**, *3*, 799.
7. Kim, I. L.; Mauck, R. L.; Burdick, J. A. *Biomaterials* **2011**, *32*, 8771.
8. Mahmoudifar, N.; Doran, P. M. *Trends Biotechnol.* **2012**, *30*, 166.
9. Remya, N. S.; Prabha, D. *Nair. Mater. Sci. Eng. C* **2013**, *33*, 575.
10. Temenoff, J. S.; Mikos, A. G. *Biomaterials* **2000**, *21*, 431.
11. Chung, C.; Burdick, J. A. *Adv. Drug. Deliv. Rev.* **2008**, *60*, 243.
12. Nguyen, L. H.; Kudva, A. K.; Guckert, N. L.; Linse, K. D.; Roy, K. *Biomaterials* **2011**, *32*, 1327.
13. El-Ayoubi, R.; DeGrandpré, C.; DiRaddo, R.; Lavigne, P.; Yousefi, A. M. *J. Biomater. Appl.* **2009**, *1*,429.
14. El-Ayoubi, R.; Eliopoulos, N.; Diraddo, R.; Galipeau, J.; Yousefi, A. M. *Tissue Eng. Part A* **2008**, *14*, 1037.
15. Ng, R.; Zang, R.; Yang, K. K.; Liu, N.; Yang, S. T. *RCS Adv.* **2012**, *2*, 10110.
16. Tang, Y. W.; Won, C.; Wang, H. X.; Alessandra. S.; Kirkland M.; Wang, X. G.; Lin T. *Tissue Eng. Part C Methods* **2011**, *17*, 209.
17. Wilhelm, A.; Hilmar, F. In Handbook of Nonwoven Fabrics; Walter, K., Eds.; Wiley-VCH: Weinheim, Germany, **2003**; Vol. *2*, Chapter 2, p 1.
18. Ghasemi-Mobarakeh, L.; Prabhakaran, M. P.; Morshed, M.; Nasr-Esfahani, M. H.; Ramakrishna, S. *Biomaterials* **2008**, *29*, 4532.
19. Ateshian, G. A.; Soslowsky, L. J.; Mow, V. C. *J. Miomech.* **1991**, *24*, 761.
20. Kladny, B.; Martus, P.; Schiwy-Bochat, K. H.; Weseloh, G.; Swoboda, B. *Int. Orthop.* **1999**, *23*, 264.
21. Kock, L.; van Donkelaar, C. C.; Ito, K. *Cell Tissue Res.* **2012**, *347*, 613.
22. Ikada, Y. J. R. *Soc. Interface* **2006**, *3*, 589.
23. Sengupta, S.; Majumdar, P. K.; Ray, P. *India J Fiber Text.* **2008**, *33*, 139.
24. Lupu, I. G.; Cramarius, O.; Hogas, H. I.; Hristian, L. *J. Text. I.* **2013**, *104*, 1125.
25. Li, Y.; Ma, T.; Yang, S. T.; Kniss, D. A. *Biomaterials* **2001**, *22*, 609.
26. Janicki, J. *Fibers Text. East. Eur.* **2011**, *19*, 66.
27. Sutherland, F. W.; Perry, T. E.; Yu, Y.; Sherwood, M. C.; Rabkin, E.; Masuda, Y.; Mayer, J. E. *Circulation* **2005**, *111*, 2783.
28. Yim, E. K.; Liao, I. C.; Leong, K. W. *Tissue Eng.* **2007**, *13*, 423.
29. Sandell, L. J.; Aigner, T. *Arthritis Res.* **2001**, *3*, 107.
30. Puppi, D.; Chiellini, F.; Piras, A. M.; Chiellini, E. *Prog. Polym. Sci.* **2010**, *35*, 403.
31. Jena, A.; Gupta, K. *Fluid Part. Sep. J.* **2002**, *14*, 227.
32. Jena, A.; Gupta, K. *Int. Nonwovens J.* **2005**, *14*, 25.
33. Midha, V. K.; Mukhopadyay A. *India J. Fiber Text* **2005**, *30*, 218.
34. Nakata, K.; Fujii, K.; Ohkoshi, Y.; Gotoh, Y.; Nagura, M.; Numata, M.; Kamiyama, M. *Macromol. Rapid. Commun.* **2007**, *28*, 792.
35. Chen, M.; Patra, P. K.; Lovett, M. L.; Kaplan, D. L.; Bhowmick, S. *J. Tissue Eng. Regen. Med.* **2009**, *3*, 269.
36. Tabata, Y.; Takahashi, Y. *J. Biomat. Sci Pol. E* **2004**, *15*, 41.
37. Nuernberger, S.; Cyran, N.; Albrecht, C.; Redl, H.; Vécsei, V.; Marlovits, S. *Biomaterials* **2011**, *32*, 1032.
38. Woodfield, T. B. F.; Blitterswijk, C. V.; Wijn, J. D.; Sims, T. J.; Hollander, A. P.; Riesle, J. *Tissue. Eng.* **2005**, *11*, 1297.

39. Klein, T. J.; Malda, J.; Sah, R. L.; Hutmacher, D. W. *Tissue Eng. Part B Rev.* **2009**, *15*, 143.

40. Chung, J. H.; Lee, S. G.; Kang, T. J. *J. Korean Fiber Soc.* **1999**, *36*, 372.

41. Ganguly, P. K.; Sengupta, S.; Samajpati, S. *India J Fiber Text.* **1999**, *24*, 34.

42. Mendonça, R. H.; de Oliveira Meiga, T.; da Costa, M. F.; da Silva Moreira Thiré, R. M. *J. Appl. Polym. Sci.* **2012**, *129*, 614.

43. O'Brien, F. J.; Harley, B. A.; Yannas, I. V.; Gibson, L. *J. Biomater.* **2005**, *26*, 433.

44. Griffon, D. J.; Sedighi, M. R.; Schaeffer, D. V.; Eurell, J. A.; Johnson, A. L. *Acta Biomater.* **2006**, *2*, 313.

45. Dedov, A. V. *Fiber Chem.* **2009**, *14*, 41.

46. Anandjiwala, R. D.; Bogualavaky, L. *Text. Res. J.* **2008**, *78*, 614.

47. Meng, Z. X.; Zheng, W.; Li, L.; Zheng, Y. F. *Mater. Chem. Phys.* **2011**, *125*, 606.

48. Natarajan, V.; Krithica, N.; Madhan, B.; Sehgal, P. K. *J. Biomed. Mater. Res. B* **2013**, *101*, 560.

49. Correia, C. R.; Moreira-Teixeira, L. S.; Moroni, L.; Reis, R. L.; van Blitterswijk, C. A.; Karperien, M.; Mano, J. F. *Tissue Eng. Part C Methods* **2011**, *17*, 717.

50. Kempson, G. E.; Tuke, M. A.; Dingle, J. T.; Barrett, A. J.; Horsefield, P. H. *BBA Gen. Subjects.* **1976**, *428*, 741.

51. Bader, D. L.; Kempson, G. E.; Barrett, A. J.; Webb, W. *BBA Gen. Subjects.* **1981**, *677*, 103.

52. Akizuki, S.; Mow, V. C.; Müller, F.; Pita, J. C.; Howell, D. S.; Manicourt, D. H. *J. Orthop.* **1986**, *4*, 379.

53. Huang, C. Y.; Stankiewicz, A.; Ateshian, G. A.; Mow, V. C. *J. Biomech.* **2005**, *38*, 799.

54. Jurvelin, J. S.; Buschmann, M. D.; Hunziker, E. B. *J. Biomech.* **1997**, *30*, 235.

55. Cartmell, S. H.; Porter, B. D.; García, A. J.; Guldberg, R. E. *Tissue Eng.* **2003**, *9*, 1197.

56. Little, C. J.; Bawolin, N. K.; Chen, X. *Tissue Eng. B* **2011**, *17*, 213.

57. Elliott, D. M.; Guilak, F.; Parker Vail, T.; Wang, J. Y.; Setton, L. A. *J. Orthop. Res.* **1999**, *17*, 503.

58. Athanasiou, K. A.; Agarwal, A.; Dzida, F. J. *J. Orthop. Res.* **1994**, *12*, 340.

59. Mow, V. C.; Guo, X. E. *Annu. Rev. Biomed. Eng.* **2002**, *4*, 175.